Journal of Theoretical Biology 483 (2019) 109989

Contents lists available at ScienceDirect

Journal of Theoretical Biology

journal homepage: www.elsevier.com/locate/jtb

Dynamic vessel adaptation in synthetic arteriovenous networks

Thierry Fredrich*, Michael Welter, Heiko Rieger

Saarland University, Center for Biophysics & Dept. Theoretical Physics, Saarbrücken 66123, Germany

ARTICLE INFO

Article history:
Received 22 May 2019
Revised 27 August 2019
Accepted 30 August 2019
Available online 31 August 2019

Keywords:
Vascular response
Capillary bed radii regulation
Blood vessel radii change in networks
Optimal capillary volume density

ABSTRACT

Blood vessel networks of living organisms continuously adapt their structure under the influence of hemodynamic and metabolic stimuli. For a fixed vessel arrangement, blood flow characteristics still depend crucially on the morphology of each vessel. Vessel diameters adapt dynamically according to internal and external stimuli: Endothelial wall shear stress, intravascular pressure, flow-dependent metabolic stimuli, and electrical stimuli conducted from distal to proximal segments along vascular walls. Pries et al. formulated a theoretical model involving these four local stimuli to simulate long-term changes of vessel diameters during structural adaption of microvascular networks. Here we apply this vessel adaptation algorithm to synthetic arteriovenous blood vessel networks generated by our simulation framework "Tumorcode". We fixed the free model parameters by an optimization method combined with the requirement of homogeneous flow in the capillary bed. We find that the local blood volume, surface to volume ratio and branching ratio differs from networks with radii fulfilling Murray's law exactly to networks with radii obtained by the adaptation algorithm although their relation is close to Murray's law.

1. Introduction

Life depends crucially on the efficiency of transport networks and therefore it is essential to understand how they are functioning and why they are efficient (Banavar et al., 1999). In particular, the vasculature of all mammalians demonstrates how nature efficiently transports and distributes nutrients at minimal costs.

Cecil Murray observed blood vessel networks in 1926 and proposed a formula describing observations on the thickness of the branches (Murray, 1926). In his theoretical derivation of the formula, he considered two energies with opposed dependency on the vessel radius r: the energy required to drive the flow and the energy required to maintain the metabolic demands of the surrounding tissue. To drive the flow, the system needs to overcome the viscous drag that is proportional to $1/r^4$ in case of Hagen–Poiseuille flow and to maintain the metabolic demands, a constant volume of "fresh" blood is required in a first approximation. By minimizing the sum of these two energies, he found that the sum of the cubes of the daughter vessel's radii equals the cube of a parent vessel's radius. In case of a simple junction with one mother vessel of radius r_c and two daughter vessels of radius r_a and r_b, this reduces to:

$$r_c^3 = r_a^3 + r_b^3 \tag{1}$$

Since his assumptions are rather general, they hold true for the respiratory system of animals and insects, xylem in plants and diverse other kinds of transport networks as well (Stephenson et al., 2015). Murray's law is based on an optimality criterion and suggests the intriguing question how the vasculature of living organisms achieves this optimality? The blood vessel wall is formed by endothelial cells with a surrounding layer of smooth muscle cells. Because the muscular layer adjusts the vessel caliber continuously during growth, maturation, in response to exercise, wound healing and diseases, the vasculature is non-stationary with regulatory mechanisms that are still under investigation. While the vascular reactions to shear stress have been known for a long time (Thoma, 1893; Wetterdal, 1920), recent studies showed that: 1) The shear stress is linked to the local intravascular pressure (Pries Axel R. et al., 1995); 2) the vascular diameter is controlled by the metabolic needs of the tissue (local oxygen partial pressure, metabolic signaling substances) (Adair et al., 1990; Berne, 1964; Berne et al., 1983; Björnberg et al., 1989) and the metabolites remaining in blood after the exchange (Ellsworth, 2004); 3) electrical signals are conducted along the blood vessel wall by endothelial and smooth muscle cells via gap junctions (Segal and Duling, 1986; de Wit et al., 2003; Bagher and Segal, 2011) and 4) in case of hypertension, the vasculature switches to inward remodeling (Jacobsen et al., 2003; Pries and Secomb, 2008).

* Corresponding author.
E-mail address: thierry@lusi.uni-sb.de (T. Fredrich).
URL: https://www.github.com/thierry3000 (T. Fredrich), http://www.uni-saarland.de/fak7/rieger/index.html (H. Rieger)

https://doi.org/10.1016/j.jtbi.2019.109989
0022-5193/

Beginning in 1995, Pries Axel R. et al. (1995) published a series of papers (Pries et al., 1998; 2001; 2003; Pries and Secomb, 2008; Pries et al., 2009) where they constructed a feedback loop between the discussed mechanisms and the blood vessel radii. Provided the resulting radius adaption dynamics leads to a stable state, this algorithm determines the blood vessel radii of a given network topology, in particular the relation between mother and daughter vessel radii at each junction without referring to Murray's law.

In this manuscript we explore the application of the adaptation algorithm to in silico arteriovenous networks and analyze the emerging vessel radii and blood flow characteristics. Initially, the networks created by our in-house simulation framework Tumorcode (Fredrich et al., 2018) are consistent with Murray's law. The vessel adaptation algorithm modifies each single vessel radius and we analyze the resulting distribution of radii. After validating our implementation by comparison with existing data in Section 3.1, we optimize the free model parameters for a fixed vessel network in Section 3.2 with respect to a maximally homogeneous blood flow in the capillary bed. In Section 3.3, we compare the distribution of radii from the initial networks with the one emerging after the application of the vessel adaptation algorithm to them.

2. Methods

2.1. The adaptation algorithm

Pries et al. (1998) presented a theoretical model to simulate vessel radii of arteriovenous networks. They constructed a feedback loop between the spatial position of the vessels (topology) and their biological functions including hydrodynamics, shear stress and metabolism of the surrounding tissue. For an elaborated review and some applications of the model see Secomb et al. (2012). In the following, we describe the vessel adaptation algorithm of Pries et al. (1998).

Considering a vessel of radius r during a time step Δt, its adaption or change $\Delta r = S_{tot}\, r\, \Delta t$ is proportional to the sum of five signals $S_{tot} = \sum_{i=1}^{5} S_i$ which are defined below.

S_1 - Shear stress. Based on the correlation between wall shear stress and vessel radius, the adaptation algorithm reduces the vessel radius whenever the wall shear stress (τ_w) falls below 1 dyn/cm^2 = 10^{-4} kPa and extends the radius otherwise, i.e:

$$S_1 = \log_{10}(\tau_w) \tag{2}$$

S_2 - Blood pressure. Pries Axel R. et al. (1995) studied the interaction of the transmural pressure P and the wall shear stress τ_e proposing a "pressure-shear" hypothesis

$$\tau_e(P) = 100 - 86 \exp\left(-5000\{\log_{10}[\log_{10}(P)]\}^{5.4}\right) \tag{3}$$

The functional form of the shear-pressure dependency is sigmoidally increasing from 14 dyn/cm^2 for pressures of 10 mmHg–100 dyn/cm^2 for pressures at 90 mmHg (Eq. (3)). With this

$$S_2 = -\log_{10}[\tau_e(P)] \tag{4}$$

S_3 - Metabolic demand. Similar to the idea of Murray (see Section 1 Introduction), the metabolic demand needs to be maintained at all times. Since oxygen is transported as cargo by the red blood cells (RBC), a constant volume flow of RBCs is required to sustain a constant oxygen supply. Given the volume flow of blood Q with hematocrit H, the volume flow of RBCs is HQ and maintained at a reference value Q_{ref} by the metabolic signal S_3.

$$S_3 = k_m \log_{10}\left(\frac{Q_{ref}}{HQ} + 1\right) \tag{5}$$

The definition of S_3 results in a strictly positive signal where the amplitude increases stronger for vessels with a lower flow rate ($HQ < Q_{ref}$) compared to vessels with a higher flow rate ($HQ > Q_{ref}$) than the reference flow Q_{ref}. In contrast to the biologically motivated reference flow, k_m is an unknown model parameter (compare Table 1).

Table 1
Parameters of the adaptation model. The values in the right column are used in Pries et al. (1998).

Signal	Free	Fixed
S_3	k_m	Q_{ref} = 40 nl/min
S_4	k_c	L = 1500 µm,
		S_0 = 40
S_5	k_s	

S_4 - Topological position. S_4 is sensitive to the position of the vessel within the entire network structure. The signal propagates from the capillary bed to the most upstream vessel in the arterial branch and to the most downstream vessel in the venous branch. While the downstream propagation of metabolic waste to the draining vein is reasonable, the upstream signaling is less obvious, but recent studies confirmed that vessels communicate via electrical signals within their endothelial layer (Segal and Duling, 1986; de Wit et al., 2003; Bagher and Segal, 2011). In principle the algorithm works with arbitrary number of vessels per intersection. For simplicity, we limit the discussion to Y-shaped intersections (Fig. 1) where a vessel c has two downstream connections (to vessel a of length x_a and to vessel b of length x_b) in an arterial branch and two feeding vessels (vessel a of length x_a and vessel b of

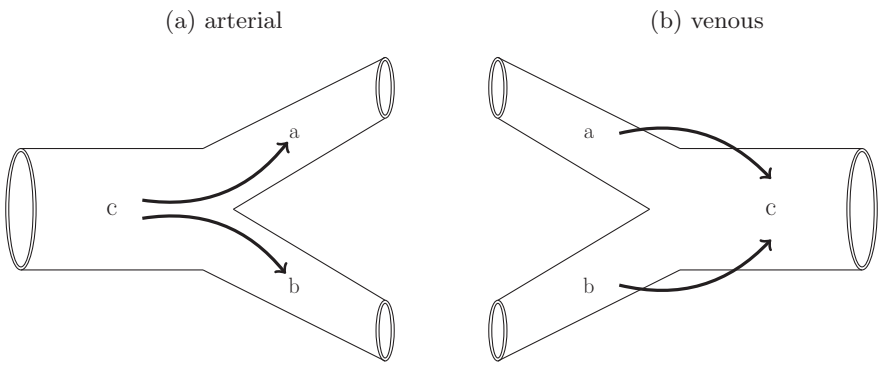

Fig. 1. Recursive propagation of the conducted signal at a vessel junction. Left: Arterial case. Right venous case. Arrows indicate the direction of information propagation. See Eq. (6).

length x_b) in a venous branch. The conducted or topological signal is calculated in a recursive fashion by the weighted sum of the metabolic signals (S_3) along the direction of information propagation (Eq. (6)). The weighting factor is proportional to the exponential of the normalized length of the vessel segments ($\frac{x_a}{L}$ and $\frac{x_b}{L}$).

$$S_{4,c} = S_{3,a} + S_{3,b} + S_{4,a}\exp(-x_a/L) + S_{4,b}\exp(-x_b/L) \tag{6}$$

Since the recursive summation might result in excessive values, the signal is damped by a reference value S_0 such that the complete conducted signal for a single vessel becomes:

$$S_4 = k_c \frac{S_{4,c}}{S_{4,c} + S_0} \tag{7}$$

Note that the constant k_c, the reference value S_0 and the normalization length L are unknown model parameters (compare Table 1).

S_5 - Shrinking tendency. The introduction of a strictly positive metabolic (S_3) and conducted signal (S_4) necessitates a negative counterbalance. Its biological motivation is the tension in the endothelial layer which leads to a contraction of the vessel radius in the absence of all other signals. In the formula of the adaptation model this is embedded by subtracting a overall constant k_s.

$$S_5 = -k_s \tag{8}$$

2.2. The artificial blood vessel networks.

We construct artificial 3D arteriovenous networks by means of our simulation framework Tumorcode (Fredrich et al., 2018). We report the complete methodology in Rieger et al. (2016) and summarize only the main steps here. First, at least one arterial and one venous root node have to be distributed in space and assigned with a hydrodynamic boundary condition (either a blood pressure value or a flow rate) before straight or Y- shape elements are appended until the arterial and venous branch merge by the capillaries. Second, the position of the capillaries within the volume is optimized towards a homogeneous capillary volume density using a hierarchical iteration scheme. For the scope of this paper, we consider only a root node configuration (RC) where one artery is opposite to one vein on the same axis (Fig. 2, compare also RC5 in Fig. 4 of Welter et al., 2016) and a single hierarchical iteration. Since the construction algorithm in the Tumorcode fixes the radii of all capillaries (2.5 µm in presented case) and determines the radii of all intermittent vessels between root nodes and capillaries by Murray's law, all radii at the intersections fulfill Murray's law by construction. Therefore we label them **M-networks** in contrast to the **A-networks** which obtain their vessel radii by applying the adaptation algorithm to the **M-networks**.

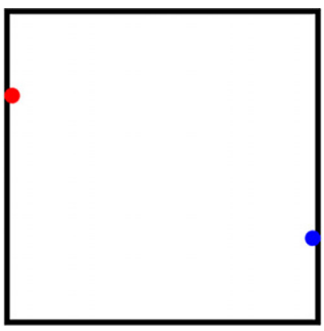

Fig. 2. Schematic root node configuration (RC) for construction the arteriovenous networks. Red (left): arterial root, blue (right): venous root.

2.3. Parameter optimization

Inspecting Section 2.1, we count six unknown model parameters as summarized in Table 1. Considering the additional hydrodynamic boundary condition at the two root nodes, we end up with 8 degrees of freedom for the model. To find the unknown parameters, we presume that a properly working vasculature requires a homogeneous flow inside the capillary bed to maintain the nutrient exchange and apply a computational optimization technique where the variance of the volume blood flow inside all capillaries ($Q_{capillaries}$) is used as cost function

$$f = Var(Q_{capillaries}) \tag{9}$$

We used particle swarm optimization (PSO) (Kennedy and Eberhart, 1995) to minimize the cost function f defined in Eq. (9). Although there is no guarantee to find the best solution, PSO finds at least a "robust" solution i.e. a solution that is robust against varying the initial conditions. In our case, the initial conditions are the values of the parameters k_m, k_c and k_s. During the PSO, we vary these parameters in the range of 0.5–4.0 for each fixed set of hydrodynamic boundary conditions. The hydrodynamic boundary conditions are the arterial inlet flow and the venous outlet pressure which we also varied in a systematic way (see supplemental text).

The numerical values of $Q_{\text{ref}} = 40$ nl/min, $L = 1500$ µm and $S_0 = 20$ were kept fix at the values reported in Pries et al. (1998).

All exact numbers, computational details and the implementation are reported in a supplemental text to this manuscript.

2.4. Definition of biophysical quantities

Given a blood vessel network inside a volume V that consists of N tubes with radii r_i and lengths l_i, two quantities of interest are the regional blood volume (rBV) and the surface to volume ratio (s2v).

2.4.1. Regional Blood Volume (rBV)

The regional blood volume measures the percentage of blood within the volume.

$$rBV = \frac{\sum_{i=1}^{N} \pi r_i^2 l_i}{V} \tag{10}$$

2.4.2. Surface to volume ratio (s2v)

The surface to volume ratio measures the ratio between the surface of an object and the volume included by this surface. Since nutrient exchange happens across the vessel surface, the exchange is proportional to the surface and therefore the s2v is an interesting quantity.

$$s2v = \frac{1}{N}\sum_{i=1}^{N} \frac{2\pi r_i l_i}{\pi r_i^2 l_i} \tag{11}$$

3. Results

3.1. Reproducing available data

We applied our implementation of the adaptation algorithm to a experimentally determined rat mesentery network. Since the hydrodynamic boundary conditions were measured, we incorporated them accordingly. The same procedure was done in Pries et al. (1998) (Network I). Unfortunately, the used time step Δt is not documented. We used $\Delta t = 0.1$ and the other adaptation parameters in Table 2. To verify our implementation, we reproduced two figures comparing the shear stress, vessel diameters, and the adaptation signals S_1, S_2, S_3 and S_4 before and after application of the algorithm.

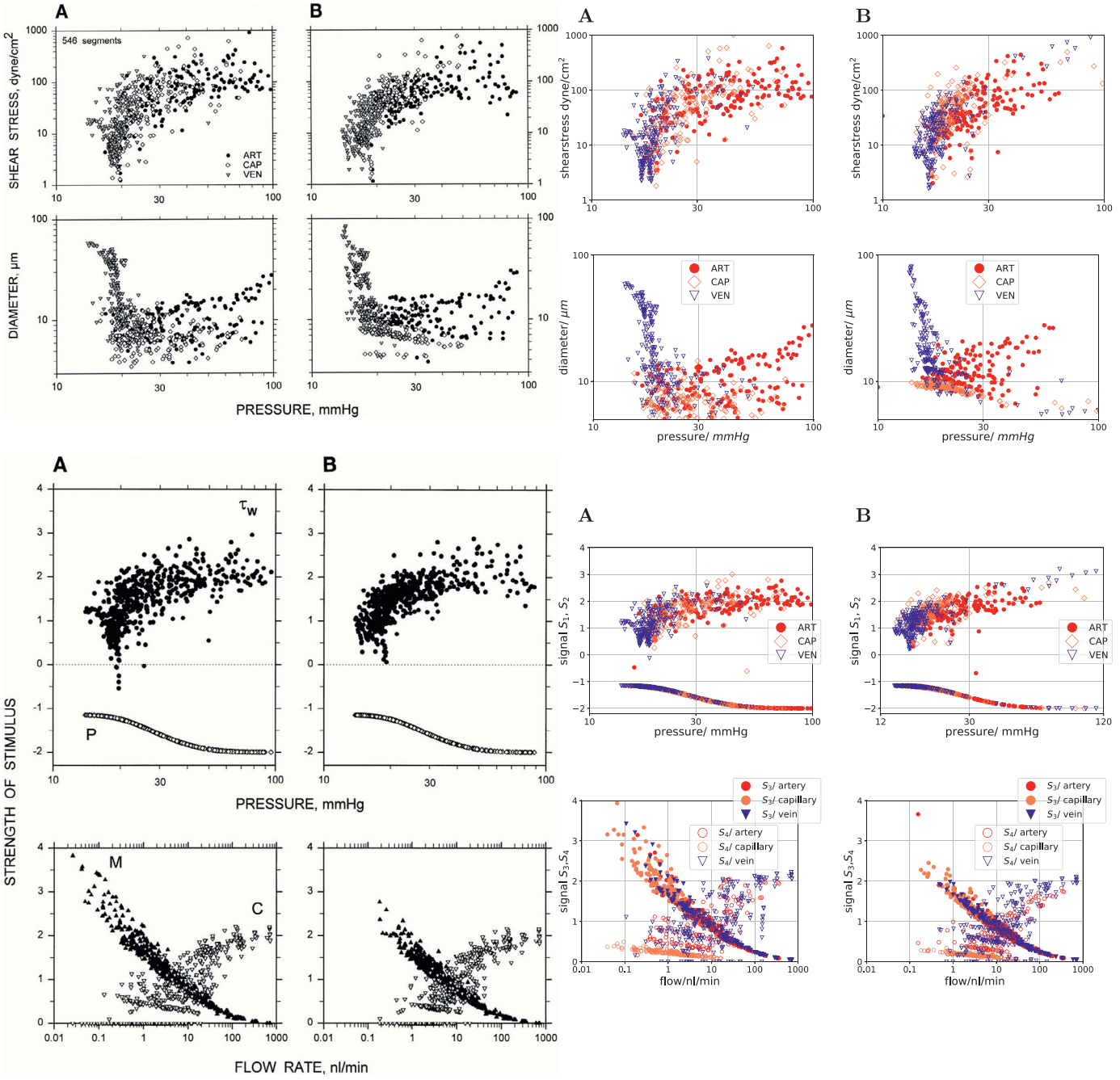

Fig. 3. Left column (black and white): reprint of Fig. 4 and 5 from Pries et al. (1998) with permission. Right column (colored): reproduced by our implementation/ software. (A): Values obtained with experimentally determined vessel diameters, (B): values obtained by simulated vessel adaptation. Top and second from top row: Distribution of shear stress and diameter for a rat mesentery network with 546 segments (162 arterioles, 167 capillaries and 217 venules). Hemodynamic parameters were calculated using the network flow model based on measured network morphology and topology. Last before bottom row: hydrodynamic stimuli derived from shear stress (τ_w) and blood pressure (P) are plotted as functions of pressure. Last row: the metabolic (M) and conducted stimuli (C) are plotted as functions of flow rate, to show functional dependence of these stimuli. (For interpretation of the references to colour in this figure legend, the reader is referred to the web version of this article.)

Table 2
Parameters used to adapt vessel radii of rat mesentery network with Tumorcode. Parameter labeled by * is not shown in Pries et al. (1998).

k_c	k_m	k_s	Q_{ref}	S_0	Δt	L
2.74	0.83	1.79	40 nl/min	20	0.1*	1500 µm

Due to the lack of quantitative data in Pries et al. (1998) we cannot compare directly, but our figures are in qualitative agreement with the original (Fig. 3). For the hydrodynamics (top row and second from top row of Fig. 3), we observe that the shear stress saturates with increasing blood pressure (top row) and the diameter varies for veins in a broader range than for the arteries with the same pressure (second row). The adaptation tends to increase the radius of the capillaries (coral labeled points in rightmost image of second row). For the distribution of the adaptation signals S_1 and S_2 (last before bottom row of Fig. 3), we find vessels in the adapted network with a higher blood pressure than 100 mmHg and therefore we extended the pressure axis (x-axis) to 120 mmHg. For the distribution of the adaptation signals S_3 and S_4 (bottom row of Fig. 3), we find that adaptation shifts the spectrum towards increased flow. In agreement with model assumptions,

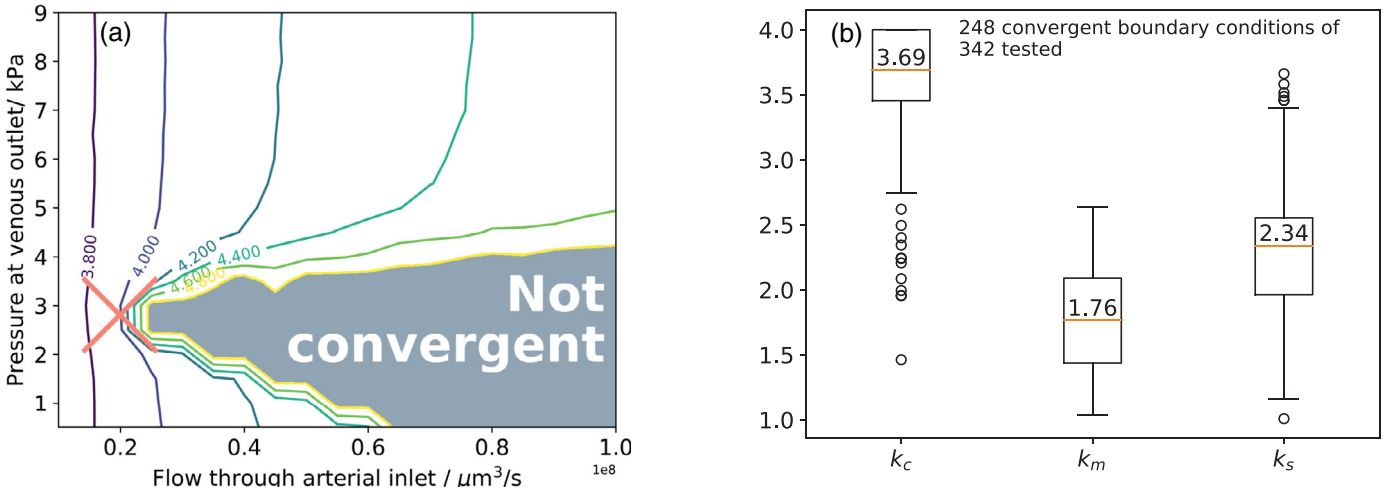

Fig. 4. Results of the particle swarm optimization (PSO). (a) Contour plot of the logarithm of the cost function f (Eq. 9) used for the PSO. x-axis: flow boundary condition at the arterial inlet. y-axis: pressure boundary condition at the venous outlet. The cross shows the boundary conditions used in Section 3.3; (b) Distribution of optimized choice for k_m, k_c and k_s. Only the convergent hydrodynamic boundary conditions are considered. The median value is write above the corresponding line.

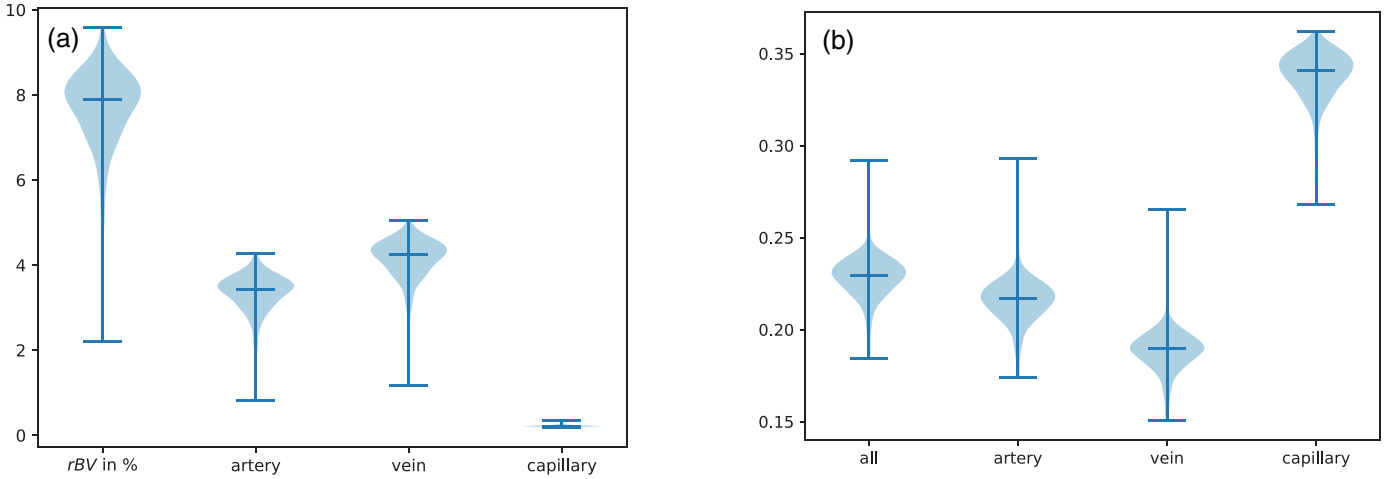

Fig. 5. Biophysical variables influenced by the adaptation algorithm. Distribution is obtained from a single configuration of vessels in space (Section 3.2), but different radii distributions obtained during particle swarm optimization. We considered the 248 convergent boundary conditions here. (a) Distribution of regional blood volume (*rBV*); (b) Distribution of surface to volume ratio (*s2v*) in 1/μm.

the metabolic signal/ demand (S_3) is higher for low flow segments and the conducted signal (S_4) increases for segments with higher flow that are more up or downstream respectively.

3.2. Single topology, varying boundary conditions

As already discussed in Pries et al. (1998), there are two possible outcomes when applying the adaptation scheme in a repeated manner: either one reaches a steady state where the changes of radii become arbitrary small with each iteration or the radii changes increase to unrealistic values which also implies unrealistic values for pressure and flow, and are not further consider.

In the remaining, we switch from the rat mesentery network to synthetic arteriovenous networks constructed by Tumorcode. We start with a single fixed topology and apply the optimization procedure described in Section 2.3. Thereby we identified the hydrodynamic boundary conditions and parameters that result in convergence of the adaptation algorithm with the fixed network topology (see Fig. 4(a)) and achieved an optimal homogeneity in the blood flow of the capillaries. Interestingly, the distribution of optimization parameters (Fig. 4(b)) indicates the same relation between the parameters ($k_m < k_s < k_c$) as found by Pries et al. in their three samples of rat mesentery networks (Pries et al., 1998).

To estimate the biological relevance of the optimized networks, we analyze two biophysical variables (Section 2.4): The regional blood volume (Fig. 5(a)) and the surface to volume ratio (Fig. 5(b)). The total regional blood volume varies within a physiological regime from 2% up to 10% (left column in Fig. 5(a)). To estimate the contributions from arteries, capillaries and veins to the total rBV, we segmented them in Fig. 5(a).

The results for the surface to volume ratio are shown in similar fashion (Fig. 5(b)). As expected, the surface to volume ratio is highest for small capillaries, smaller for arteries and the smallest for the large veins.

3.3. Varying topology, fixed boundary conditions

In contrast to the previous section, we now 1) keep the hydrodynamic boundary conditions and adaptation parameters fixed and 2) vary the topological arrangement of the vessels i.e. we

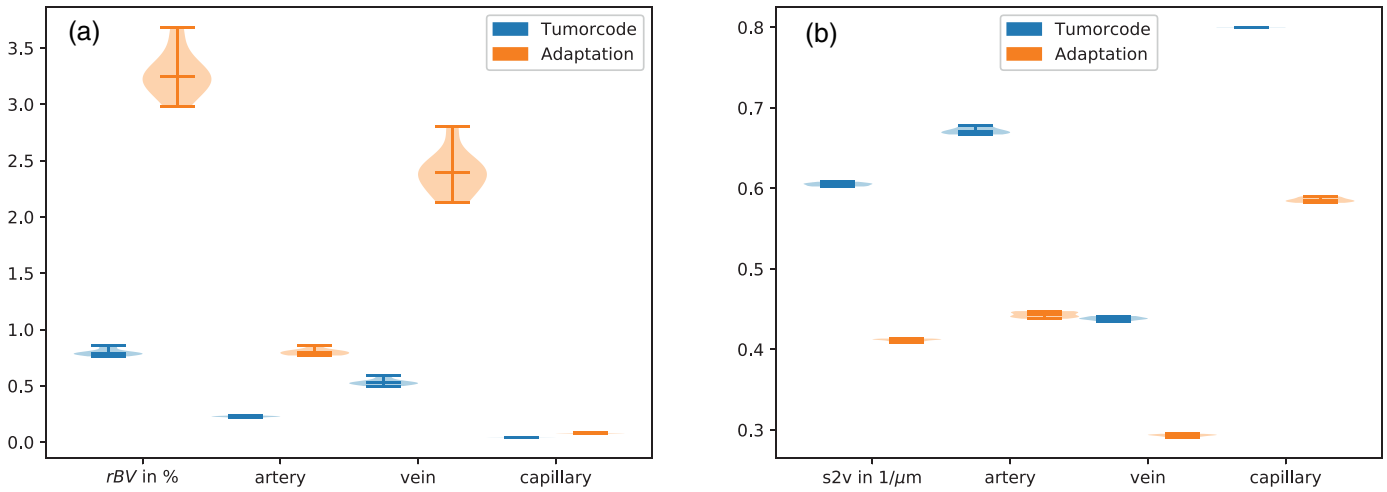

Fig. 6. Biophysical variables influenced by the adaptation algorithm. Distribution is taken from 10 different arrangements of vessels in space with radii obtained by 1) construction by Tumorcode (blue) and 2) application of the adaptation algorithm with a fixed set of parameters (Table 2, orange). (a) Distribution of regional blood volume (*rBV*); (b) Distribution of surface to volume ratio (*s2v*) in 1/μm. (For interpretation of the references to colour in this figure legend, the reader is referred to the web version of this article.)

Table 3
Mean value and standard error of the mean for rBV and s2v averaged over the 10 considered networks.

		All types	Artery	Vein	Capillary
rBV	Tumorcode	0.80 ± 0.03	0.227 ± 0.006	0.532 ± 0.03	0.039 ± 0.001
	Adaptation	3.3 ± 0.2	0.80 ± 0.03	2.4 ± 0.2	0.076 ± 0.003
s2v	Tumorcode	0.605 ± 0.002	0.672 ± 0.004	0.439 ± 0.002	0.8*
	Adaptation	0.412 ± 0.001	0.443 ± 0.003	0.293 ± 0.002	0.586 ± 0.003

* Note that the radius of a capillary is fixed in synthetic networks constructed by Tumorcode.
Data also visualized in Fig. 6.

grow different networks with same root node configuration. Based on the results of the PSO (red cross in Fig. 4(a)), we decided to use a pressure of 2.8 kPa at venous outlet and a volume flow rate of $2 \cdot 10^7$ μm^3/s at the arterial inlet to create 10 independent realizations of arteriovenous networks (**M-networks**) of lateral size 1500 μm (see Section 2.2).

3.3.1. Biophysical quantities

We apply the adaptation algorithm with the parameter set listed in Table 2 to the 10 samples. Hence we constructed 10 **A-networks** which we compare regarding their regional blood volume rBV (Fig. 6(a)) and their surface to volume ratio s2v (Fig. 6(b)) to the **M-networks** (numerical values listed in Table 3).

For the **A-networks**, the overall rBV is more than 4 times higher than for the **M-networks** (left column of Fig. 6(a)). In each case, the contribution of the veins to the rBV is the highest (66% for Tumorcode and 72% for Adaptation). For the **M-networks**, the overall s2v ratio is about 1.5 times higher than for the **A-networks** (left column of Fig. 6(b)). The s2v is highest at the capillary bed followed by the arteries and the veins.

The observed behavior follows from the hierarchical structure of the vascular network. Considering a fixed volume and vessels with fixed segment length (as in our case), the s2v scales proportional to the inverse of the radius and the rBV scales proportional to the vessel radius squared (Section 2.4). Since capillaries are smaller than arteries and veins in a hierarchical structure, the s2v increases and the rBV decreases when going from the upper (artery, vein) to the lower level (capillary), as observed.

Essentially, the **M-networks** feature systematically smaller vessel radii increasing the s2v ratio at the cost of higher flow resistance.

3.3.2. Adaptation signals

Similar to Fig. 3, we plot: a) The hydrodynamic characteristics (top and next to top row in Fig. 7), b) the hydrodynamic signal (last before bottom row in Fig. 7), and c) the conducted and metabolic signals (bottom row in Fig. 7) for one representative of the **A-networks** in Fig. 7. For the other nine networks, the plots look qualitatively similar.

Before adaptation, there is no correlation between the wall shear stress and the pressure, and since the signal S_1 (positive values of last before bottom row) depends only on the logarithm of the shear stress, there is also no functional dependence of S_1 on the pressure. After the adaptation however, the dependence of the shear stress and the signal S_1 on the pressure becomes more pronounced (right column of Fig. 7): Veins approach a plateau with increasing pressure and the arteries with decreasing pressure. For the shear stress, the plateau is between 50–100 dyn/cm^2 and for the signal S_1 around 2. The diameter depends on the pressure as expected for our networks: starting with the vessels of the smallest diameter (the capillaries), the diameter increases as we raise the pressure along the arterial branch and decrease the pressure along the venous branch (second row of Fig. 7). The negative values in the last before bottom row of Fig. 7 present the signal S_2 (Eq. 4). Here we notice that the values for S_2 are more restricted for veins (between −1.2 and −1.7) than for arteries (between −1.1 and −2.0). The metabolic and conducted signal (bottom row of Fig. 7) shift their maximum / minimum from 0.01 nl/min to increased flows at about 1 nl/min.

3.3.3. Visual inspection

Although the distribution of radii changes from the **M-networks** (bottom left of Fig. 8) to **A-networks** (bottom right

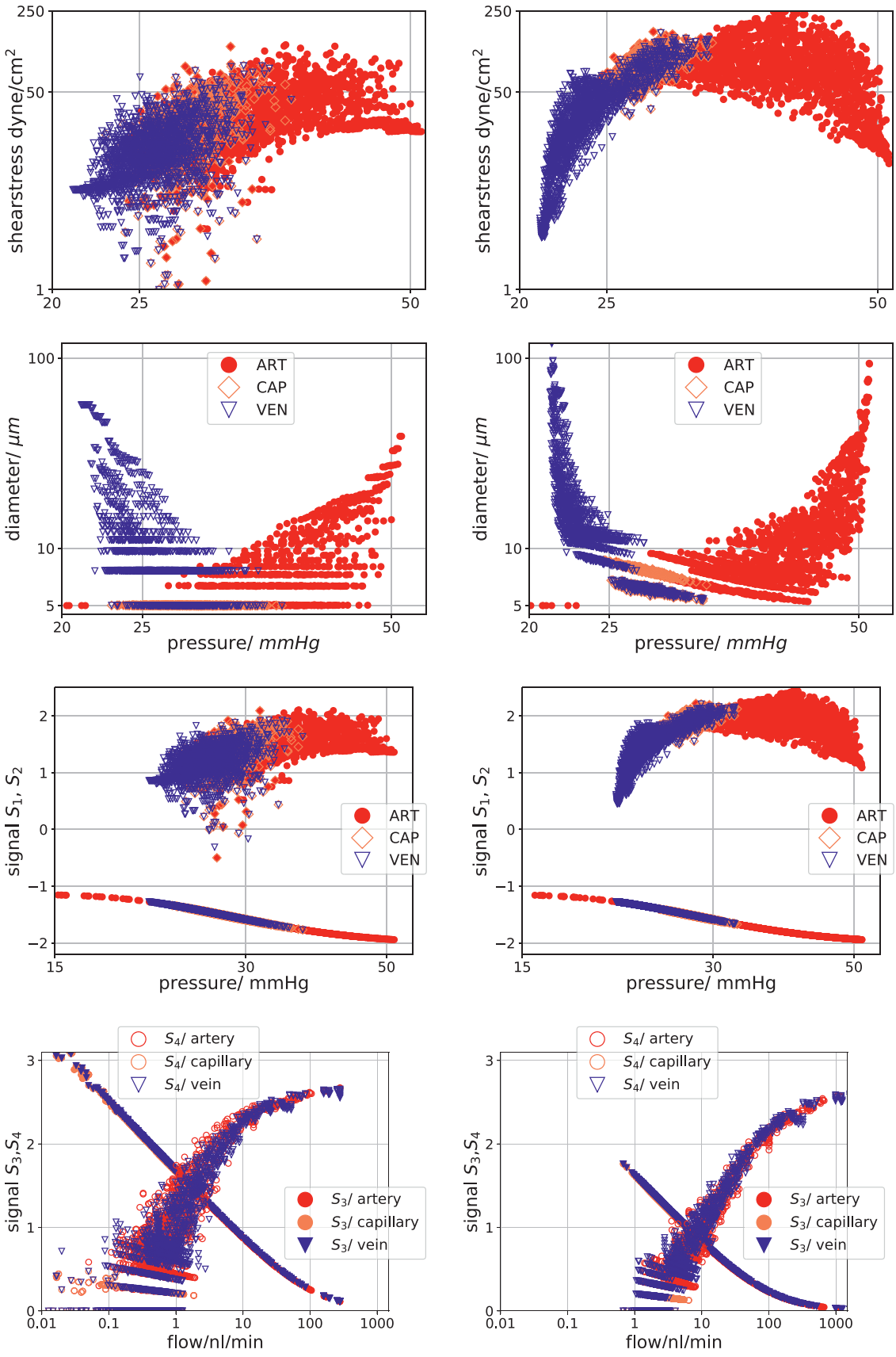

Fig. 7. The characteristics for a single arteriovenous network. Left column: Without adaptation. Right column: convergent adaptation with parameters listed in Table 2. A graphical representation of this particular network is shown in Fig. 8. From top to bottom we compare the shear stress, the vessel diameter, the hydrodynamic signals (S_1 and S_2 of Section 2.1) and the metabolic and conducted signal (S_3 and S_4 of Section 2.1). (For interpretation of the references to colour in this figure legend, the reader is referred to the web version of this article.)

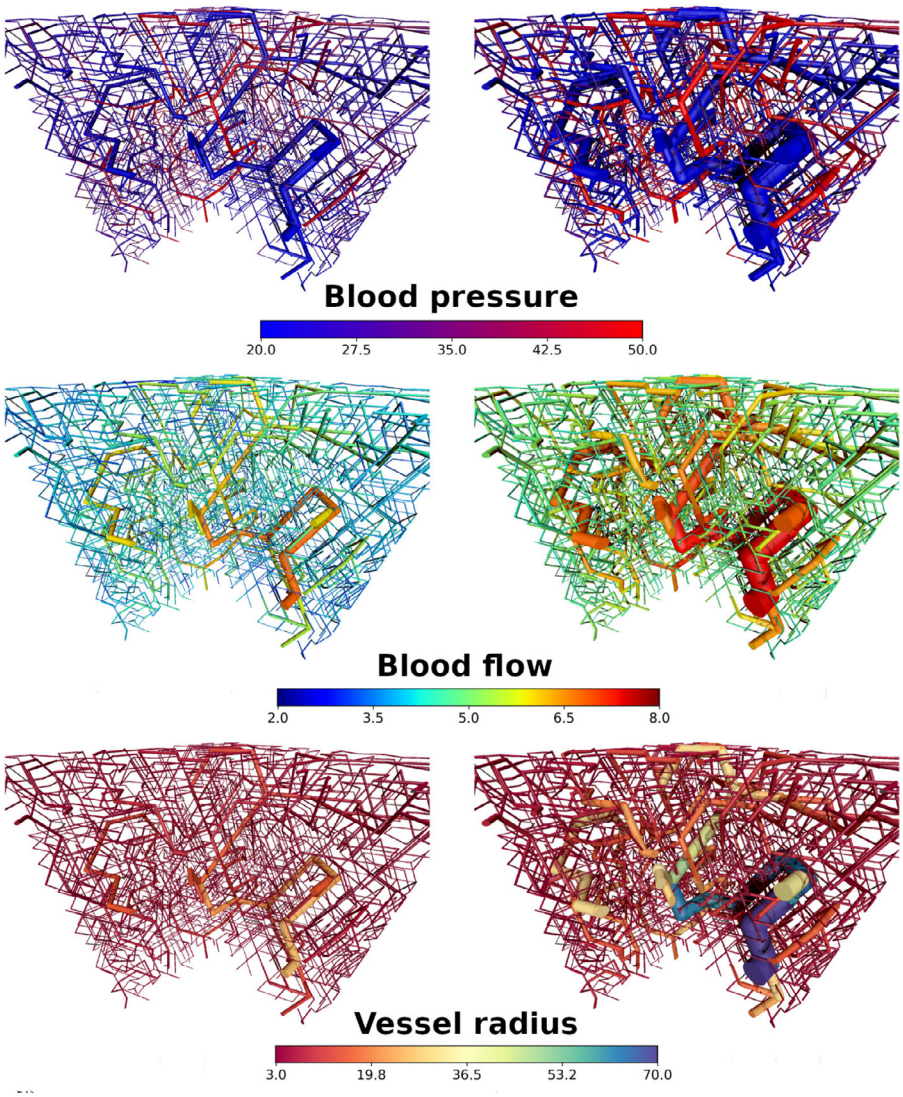

Fig. 8. Color coded vessel properties for one representative of the ensemble of synthetic arteriovenous networks. Left column: radii distribution from Tumorcode (Murray's law). Right column: Radii distribution after adaptation. From top to bottom: Pressure in mmHg, volume flow (logarithmic scale) in $\mu m^3/s$, radius in µm. (For interpretation of the references to colour in this figure legend, the reader is referred to the web version of this article.)

column of Fig. 8), the distribution of the blood pressure does not change because of the fixed boundary conditions (colors of top row in Fig. 8). The shear force is proportional to the flow and therefore the distribution of the shear force looks similar to the distribution of flow as show in the center row of Fig. 8. In the bottom row of Fig. 8, we colored the vessel by their radii to highlight changes of the vessel radii by the adaptation algorithm.

Finally, Fig. 9 shows data that is only available in the adaptation case (metabolic signal and conducted signal). In agreement with model assumptions, the metabolic signal is highest at the thin capillaries and the conducted signal is highest at the most distal points.

3.4. Murray's law

The networks created by Tumorcode fulfill Murray's law by construction (Section 2.2). Here we check for a single network (shown in Fig. 8) whether it still fulfills Murray's law after the application of the adaptation algorithm.

In Fig. 10 we plot for each bifurcation the cubic root of the sum of daughter vessel radii cube against the radius of the mother vessel. If the mother and daughter vessel radii would fulfill Murray's law, the data points would lie on the straight line, which they do remarkably closely. Applying Murray's law locally at each bifurcation in large networks results in a complicated dependence of the vessel radius on the global vessel arrangement. Nevertheless the distribution of the differences between the radii of two daughter vessels in **M-networks** displays characteristic features like discrete peaks at specific difference values, as shown in Fig. 11. This can be understood as follows: since the network construction algorithm of Tumorcode uses a fixed capillary radius and a discrete vessel length (on a lattice), repeated application of Murray's law leads more often to the same proportions at an intersection. To illustrate this, we use a hypothetical capillary bed as shown in Fig. 12. For the bifurcations b_1, b_2 and b_3 (Fig. 12), we calculate the quantity used in the histogram shown in Fig. 11: The differences of the daughter vessel radii normalized by the mother vessel radius.

b_1	b_2	b_3
$\frac{2.5\mu m - 2.5\mu m}{3.15\mu m} = 0.0$	$\frac{3.15\mu m - 2.5\mu m}{3.61\mu m} = 0.18$	$\frac{3.61\mu m - 2.5\mu m}{3.97\mu m} = 0.28$

The three highest peaks of the histogram are located around the calculated values (0.0, 0.18 and 0.28).

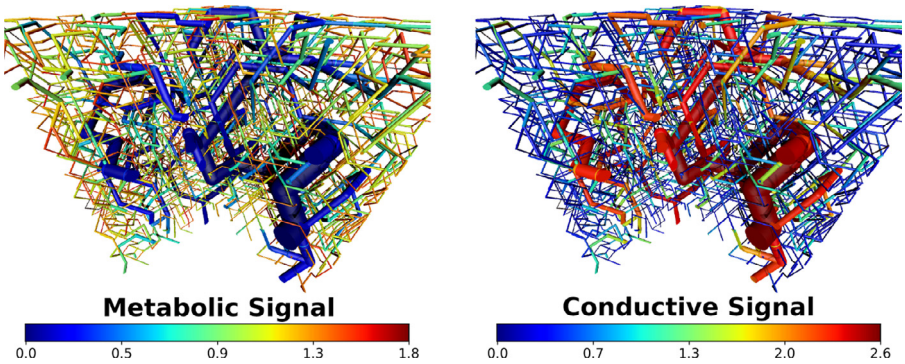

Fig. 9. Adaptation signals (Section 2.1) for one representative of the ensemble of synthetic arteriovenous networks. Left column: Metabolic signal (S_3) Right column: conducted signal (S_4). (For interpretation of the references to colour in this figure legend, the reader is referred to the web version of this article.)

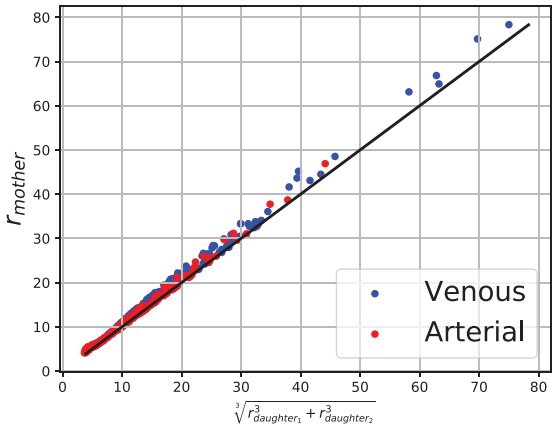

Fig. 10. The black diagonal represents Murray's law for $\alpha = 3$. The data points are taken from the A-network shown in Fig. 8 in the right column. Blue dots are venous intersections (431) and red dots are arterial intersections (475). (For interpretation of the references to colour in this figure legend, the reader is referred to the web version of this article.)

On the other hand, the distribution of the differences between the radii of daughter vessels in **A-networks** is much smoother and lacks discrete peaks. The adaptation algorithm adjusts each vessel radius and removes the initial vessel radii discretization, resulting in a radii distribution in **A-networks** that differs significantly from **M-networks**. The more remarkable is the observation that the radii still obey Murray's law very closely.

4. Discussion

We compared arteriovenous networks constructed by the Tumorcode (**M-networks**, radii obey Murray's law by construction) with networks having the same topology, but with vessel radii obtained by the adaptation algorithm (**A-networks**).

The most interesting result is that structural adaptation leads to a network that differs significantly from one generated by strict application of Murray's law, yet the adapted network satisfies Murray's law quite closely. Small but systematic deviations from Murray's law at each bifurcation level (compare Fig. 10) accumulate over subsequent levels and result in generally larger vessel radii in **A-networks** compared to **M-networks** and consequently in global differences in regional blood flow (rBV) and surface to volume ratio (s2v). A quantitative analysis of rBV (Fig. 5(a), 6(a) and Table 3) and s2v (Fig. 5(b), 6(b) and Table 3) confirms that the **A-networks** carry more blood while the **M-networks** show a higher surface to volume ratio — especially at the capillary level — at the expense of an elevated flow resistance.

Moreover, the adaptation algorithm smoothens the distribution of the differences of the radii of the two daughter vessels at each

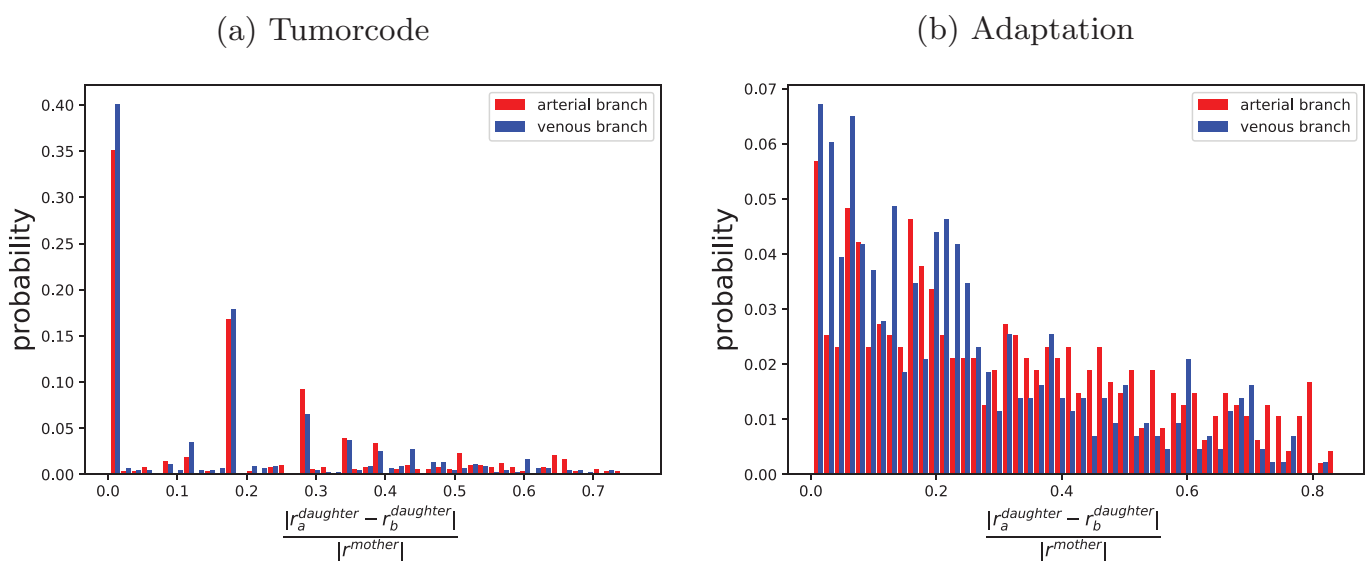

Fig. 11. Normalized distribution of differences between two daughter vessels at a Y- shaped intersection. The used topology is the same for both cases and shown in Fig. 8. Left column: before adaptation (vessel radii fulfilling Murray's law by construction in Tumorcode). Right column: same topology as left column but vessel radii adapted with parameter set listed in Table 2. (For interpretation of the references to colour in this figure legend, the reader is referred to the web version of this article.)

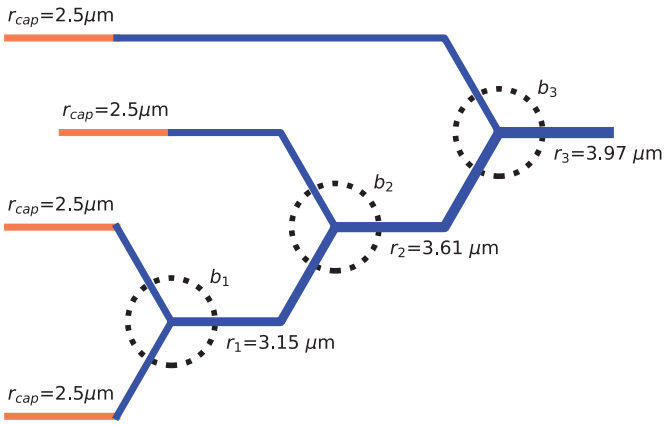

Fig. 12. Schematic view on capillary bed as constructed by the Tumorcode Software. The vessels indicated in coral are capillaries with radius r_{cap}=2.5 μm. At bifurcation b_1, b_2 and b_3 the upstream vessel radii r_1, r_2 and r_3 are calculate by Murray's law with exponent 3. (For interpretation of the references to colour in this figure legend, the reader is referred to the web version of this article.)

bifurcation. This observation demonstrates that for a given network topology more than one radii distribution can fulfill Murray's law, at least very closely. The reproduction of Murray's law by structural adaptation is particularly remarkable since the algorithm produces radii variation due to signals involving chemical energy (metabolic signal), the tension of endothelial layer (shrinking tendency) and non-local contributions (conducted signal). It is interesting to find a relation close to Murray's law although drag and flow are not directly used in the adaptation model. Instead, our choice of the objective function in the optimization procedure (Section 2.3) is based on a requirement for optimal homogenization of the capillary flow. Among several other objective functions, we found that minimizing the overall variance of the capillary flow achieves convergence of the adaptation algorithm for our synthetic arteriovenous networks.

It would be interesting to study structural adaptation in the case of pathological networks such as blood vessel networks modified by a growing tumor (Carmeliet and Jain, 2000), involving angiogenesis, vessel regression and collapse. We tried to include the adaptation algorithm into our model of tumor vascularization (Welter and Rieger, 2010; Rieger et al., 2016; Welter et al., 2016), implemented in Tumorcode (Fredrich et al., 2018). Using a convergent set of adaptation parameters for a given arteriovenous network (as analyzed in this manuscript), the convergence was not achieved when the network topology is subsequently altered during tumor growth. The potential reasons for the failure of convergence are analyzed in a supplemental text. A successful application of the adaptation algorithm in the presence of vascular remodeling was reported in Secomb et al. (2013): Angiogenesis combined with vascular pruning based on low oxygen saturation resulted in stable radii distributions. The application of structural adaptation amended by angiogenesis and pruning to vascular remodeling in growing tumors is topic of future research. So far, there seems to be no consensus in the field how to include structural adaptation into vascular tumor growth. The discussion of the stability of networks with low generation shunts in the appendix of Pries et al. (1998) proves that the adaptation algorithm cannot be stable without the conducted signal. However, some mathematical models of vascularized tumor growth include vessel radius adaptation (McDougall et al., 2006), but no conducted signal, although it is an integral component of the structural adaptation theory, at least in the non-cancerous setting.

The signals introduced by the adaptation algorithm are based on biological relevant processes which provide an input for mathematical modeling. Currently the signals are modeled with parameters (compare Table 1), but in the future the variations in endothelial cell membrane potential along a vessel or its metabolic uptake might become experimentally measurable fixing the free parameters of the adaptation model used here.

5. Data availability

We support open science by sharing our software and the created raw data at www.zenodo.org.

5.1. Software

A developer version of the Tumorcode software tool (Fredrich et al., 2018) is hosted at www.github.com/thierry3000/tumorcode. For the presented manuscript, we worked with the Pre-release v1.1.0-alpha.1 (Adaptation) version of the code which we also archived (Fredrich and DaWelter, 2019).

5.2. Data

We store the results of executed simulations, the used settings and parameters, the network topologies and the images in a single compressed archive (Fredrich, 2019).

Acknowledgment

We thank Adam Wysocki for useful discussions and acknowledge financial support by the DFG (German Research Foundation) via the Collaborative Research Center SFB 1027.

Supplementary material

Supplementary material associated with this article can be found, in the online version, at doi:10.1016/j.jtbi.2019.109989.

References

Adair, T.H., Gay, W.J., Montani, J.P., 1990. Growth regulation of the vascular system: evidence for a metabolic hypothesis. Am. J. Physiol.-Regul. Integr. Compar. Physiol. 259 (3), R393–R404. doi:10.1152/ajpregu.1990.259.3.R393.

Bagher, P., Segal, S.S., 2011. Regulation of blood flow in the microcirculation: role of conducted vasodilation. Acta physiologica (Oxford, England) 202 (3), 271–284. doi:10.1111/j.1748-1716.2010.02244.x.

Banavar, J.R., Maritan, A., Rinaldo, A., 1999. Size and form in efficient transportation networks. Nature 399 (6732), 130–132. doi:10.1038/20144.

Berne, R.M., 1964. Metabolic regulation of blood flow. Circul. Res. 15, SUPPL:261–268.

Berne, R.M., Knabb, R.M., Ely, S.W., Rubio, R., 1983. Adenosine in the local regulation of blood flow: a brief overview. Feder. Proc. 42 (15), 3136–3142.

Björnberg, J., Maspers, M., Mellander, S., 1989. Metabolic control of large-bore arterial resistance vessels, arterioles, and veins in cat skeletal muscle during exercise. Acta Physiologica Scandinavica 135 (2), 83–94. doi:10.1111/j.1748-1716.1989.tb08555.x.

Carmeliet, P., Jain, R.K., 2000. Angiogenesis in cancer and other diseases. Nature 407 (6801), 249. doi:10.1038/35025220.

Ellsworth, M.L., 2004. Red blood cell–derived ATP as a regulator of skeletal muscle perfusion. Med. Sci. Sports Exer. 36 (1), 35. doi:10.1249/01.MSS.0000106284.80300.B2.

Fredrich, T., 2019. Dynamic vessel adaptation in synthetic arteriovenous networks. Technical Report. Zenodo doi:10.5281/zenodo.2710926.

Fredrich, T., DaWelter, 2019. thierry3000/tumorcode: adaptation. doi:10.5281/zenodo.2710460.

Fredrich, T., Welter, M., Rieger, H., 2018. Tumorcode. Eur. Phys. J. E 41 (4), 55. doi:10.1140/epje/i2018-11659-x.

Jacobsen, J.C.B., Gustafsson, F., Holstein-Rathlou, N.-H., 2003. A model of physical factors in the structural adaptation of microvascular networks in normotension and hypertension. Physiol. Meas. 24 (4), 891–912. doi:10.1088/0967-3334/24/4/007.

Kennedy, J., Eberhart, R., 1995. Particle swarm optimization. In: Proceedings of ICNN'95 - International Conference on Neural Networks, 4, pp. 1942–1948 vol.4. doi:10.1109/ICNN.1995.488968.

McDougall, S.R., Anderson, A.R.A., Chaplain, M.A.J., 2006. Mathematical modelling of dynamic adaptive tumour-induced angiogenesis: clinical implications and therapeutic targeting strategies. J. Theoret. Biol. 241 (3), 564–589. doi:10.1016/j.jtbi.2005.12.022.

Murray, C.D., 1926. The physiological principle of minimum work. Proc. Natl. Acad. Sci.United States Am. 12 (5), 299–304.
Pries, A.R., Cornelissen, A.J.M., Sloot, A.A., Hinkeldey, M., Dreher, M.R., Höpfner, M., Dewhirst, M.W., Secomb, T.W., 2009. Structural adaptation and heterogeneity of normal and tumor microvascular networks. PLoS Comput. Biol. 5 (5), e1000394. doi:10.1371/journal.pcbi.1000394.
Pries, A.R., Reglin, B., Secomb, T.W., 2001. Structural adaptation of microvascular networks: functional roles of adaptive responses. Am. J. Physiol. 281 (3), H1015–H1025.
Pries, A.R., Reglin, B., Secomb, T.W., 2003. Structural response of microcirculatory networks to changes in demand: information transfer by shear stress. Am. J. Physiol. 284 (6), H2204–H2212. doi:10.1152/ajpheart.00757.2002.
Pries, A.R., Secomb, T.W., 2008. Modeling structural adaptation of microcirculation. Microcirculation (New York, N.Y. : 1994) 15 (8), 753–764. doi:10.1080/10739680802229076.
Pries, A.R., Secomb, T.W., Gaehtgens, P., 1998. Structural adaptation and stability of microvascular networks: theory and simulations. Am. J. Physiol. 275 (2), H349–H360.
Pries Axel, R., Secomb Timothy, W., Peter, G., 1995. Design principles of vascular beds. Circul. Res. 77 (5), 1017–1023. doi:10.1161/01.RES.77.5.1017.
Rieger, H., Fredrich, T., Welter, M., 2016. Physics of the tumor vasculature: theory and experiment. Eur. Phys. J. Plus 131 (2), 31. doi:10.1140/epjp/i2016-16031-9.
Secomb, T.W., Alberding, J.P., Hsu, R., Dewhirst, M.W., Pries, A.R., 2013. Angiogenesis: an adaptive dynamic biological patterning problem. PLoS Comput. Biol. 9 (3), e1002983. doi:10.1371/journal.pcbi.1002983.
Secomb, T.W., Dewhirst, M.W., Pries, A.R., 2012. Structural adaptation of normal and tumour vascular networks. BasicClin. Pharmacol. Toxicol. 110 (1), 63–69. doi:10.1111/j.1742-7843.2011.00815.x.
Segal, S.S., Duling, B.R., 1986. Flow control among microvessels coordinated by intercellular conduction. Science 234 (4778), 868–870. doi:10.1126/science.3775368.
Stephenson, D., Patronis, A., Holland, D.M., Lockerby, D.A., 2015. Generalizing murray's law: an optimization principle for fluidic networks of arbitrary shape and scale. J. Appl. Phys. 118 (17), 174302. doi:10.1063/1.4935288.
Thoma, R.A., 1893. Untersuchungen über die Histogenese und Histomechanik des Gefäss-systems, von Dr R. Thoma, ... F. Enke, Stuttgart. OCLC: 458283924
Welter, M., Fredrich, T., Rinneberg, H., Rieger, H., 2016. Computational model for tumor oxygenation applied to clinical data on breast tumor hemoglobin concentrations suggests vascular dilatation and compression. PLOS ONE 11 (8), e0161267. doi:10.1371/journal.pone.0161267.
Welter, M., Rieger, H., 2010. Physical determinants of vascular network remodeling during tumor growth. Eur. Phys. J. E 33 (2), 149–163. doi:10.1140/epje/i2010-10611-6.
Wetterdal, P., 1920. Beiträge zur Morphologie des Gefässsystems: Die Entwickelung der Gefässe in der Brustflosse bei Squalus Acanthias nebst Bemerkungen über die Entwickelung der Arterien der vorderen Extremitäten im Allgemeinen. J.F. Bergmann-Verlag München.
de Wit, C., Roos, F., Bolz, S.-S., Pohl, U., 2003. Lack of vascular connexin 40 is associated with hypertension and irregular arteriolar vasomotion. Physiol. Genomics 13 (2), 169–177. doi:10.1152/physiolgenomics.00169.2002.